arXiv:cond-mat/0003247v1 [cond-mat.supr-con] 14 Mar 2000

Nonlinear electrodynamics of p-wave superconductors

Klaus Halterman* and Oriol T. Valls+
School of Physics and Astronomy and Minnesota Supercomputer Institute
University of Minnesota
Minneapolis, Minnesota 55455-0149
(February 1, 2008)

We consider the Maxwell-London electrodynamics of three dimensional superconductors in p-wave pairing states with nodal points or lines in the energy gap. The current-velocity relation is then nonlinear in the applied field, cubic for point nodes and quadratic for lines. We obtain explicit angular and depth dependent expressions for measurable quantities such as the transverse magnetic moment, and associated torque. These dependences are different for point and line nodes and can be used to distinguish between different order parameters. We discuss the experimental feasibility of this method, and bring forth its advantages, as well as limitations that might be present.

I. INTRODUCTION

The number and variety of superconducting materials for which evidence of exotic Cooper pairing (i.e., pairing in a state other than the usual s-wave) exists is constantly increasing. For high temperature superconducting oxides (HTSC's) the consensus[1] is indeed that the pairing state is, in nearly all cases, at least predominantly d-wave, specifically of the $d_{x^2-y^2}$ form, with lines of nodes. Rather persuasive (although not conclusive) evidence in the form of both experiments and theoretical arguments,[2–4] has recently been brought forward for p-wave superconductivity in $\mathrm{Sr_2RuO_4}$. The pairing state currently favored by many is of the same form[5–8] as that of the A phase[9] in ^{3}He, which has point nodes. Several heavy fermion (HF) materials, the discovery of which predated that of HTSC's but for which determinations of the pairing state have proved harder to achieve, are now also believed with varying degrees of certainty, to belong in the exotic camp[10–12]. There are also results indicating[13,14] that superconducting families of organic salts such as $\kappa-\mathrm{(BEDT-TTF)_2Cu(NCS)_2}$ and $\mathrm{(TMTSF)_2X}$ $(\mathrm{X}=\mathrm{PF_6},\mathrm{ClO_4},\text{etc.})$ also exhibit unconventional superconductivity. In some cases it has been argued that the pairing appears to be in the p-wave[15,16].

Determination of pairing states is not easy, particularly if one wishes to know more details than merely their overall symmetry. Even in the best studied HTSC's, questions such as what is the angle between lines of nodes in orthorhombic compounds, or whether true nodes, rather than very deep minima, exist, are still matters for occasionally heated debate. The situation is much worse for the other materials mentioned, where the evidence is much more preliminary, and at times contradictory.[17–22] The determination of the pairing state is often hampered by difficulties in interpreting results. Regions (points or lines) where the energy gap vanishes are often the signature of exotic pairing (but not invariably, the B phase of ^{3}He is a well-known counterexample). These "gap nodes" lead to various power law behaviors for quantities that otherwise would behave exponentially with temperature, but sometimes there are alternative explanations for the power laws. It is difficult moreover, to distinguish between experimental outcomes arising from zeroes in the energy gap and those arising only from strong anisotropy. An additional complication is that for non s-wave superconducting materials, the order parameter (OP) state at the surface may easily differ[23] from that in the bulk.

It is therefore important to study probes of the OP symmetry able to discern as unambiguously as possible details of the pairing state, such as the existence, nature and position of the *bulk* OP nodes. One such probe is afforded by the nonlinear Maxwell-London electrodynamics of exotic pairing states in the Meissner regime. Electrodynamic effects probe the sample over a scale determined by the penetration depth λ, which is large for the materials of interest. It was pointed out[24] in the context of d-wave superconductivity that order parameter nodes lead to observable nonlinear effects at low temperatures, the chief quantities of experimental interest being the magnetic field dependent penetration depth $\lambda(H)$, the nonlinear transverse component of the magnetic moment, $m_\perp$, induced by the application of a magnetic field, and the torque associated with this transverse moment.[25–27]. Further developments of the method, always in the context of predominantly d-wave superconductivity, showed[28] that it can be used to perform *node spectroscopy*, that is, to infer in detail the angular structure of the regions where the order parameter vanishes (nodes) or is very small ("quasinodes").

These developments took place within the study of the high temperature oxide superconductors. For these materials, the temperature scales as set by T_c are higher and achieving the required low temperature conditions is very easy. However, recent improvements in experimental techniques involving torsional oscillators[29] and torque magnetometry[30] make it possible to measure extremely small moments and torques at dilution refrigerator temperatures. Experiments to accurately measure λ in that temperature range are also[31] being planned. Thus, the relevant region for performing nonlinear electrodynamics experiments in low T_c materials is becoming accessible.

With this in mind, we take up in this work the question of the use of methods based on nonlinear electrodynamics to study exotic superconducting materials, other than HTSC's. Specifically, we will consider here simple OP's both with point nodes and with three-dimensional nodal lines, as would occur for example in p-wave superconductivity. Our efforts will focus on the calculation of the dependence of $m_\perp$ (or its associated torque) on the magnetic field and the appropriate angle of rotation. We also compute the field dependence of the low temperature penetration depth. We will present estimates based on published values of the relevant material parameters showing that the required measurements appear to be technically feasible. These estimates are presented, not to prejudge the pairing state associated with any material, but rather to show the expected signal *if* the material indeed does have the assumed OP.

In the next Section we introduce the geometries and the order parameter forms that we study. We then calculate the nonlinear relation between current and superfluid flow field, using an extension of the three dimensional methods of Ref. 27. From these relations, we obtain the physical quantities of interest, through the appropriate generalization of existing[28] perturbation methods. In Section III we summarize our results, and consider the question of the experimental feasibility of using this method on several materials. We conclude with a discussion of the advantages and limitations of the method and of the specific treatment presented in this work.

II. METHODS AND RESULTS

A. Maxwell-London Electrodynamics

We first briefly outline the nonlinear Maxwell-London equations, on which our method is built. We will not dwell into any details that were discussed elsewhere.[24,25,27]. When a magnetic field $\mathbf{H}_a$ is applied to a superconductor a superfluid flow field $\mathbf{v}(\mathbf{r})$ is set up. The relation between $\mathbf{v}(\mathbf{r})$ and the local magnetic field $\mathbf{H}(\mathbf{r})$ is given[32] by the second London equation:

$$\nabla \times \mathbf{v} = \frac{e}{c}\mathbf{H}. \tag{2.1}$$

where e is the proton charge. Ampère's law for steady-state currents, $\nabla \times \mathbf{H} = \frac{4\pi}{c}\mathbf{j}$, can be combined with Eq. (2.1) to obtain:

$$\nabla \times \nabla \times \mathbf{v} = \frac{4\pi e}{c^2}\mathbf{j}(\mathbf{v}). \tag{2.2}$$

In this equation there are still two unknown fields. For a solution to be obtained, the functional relationship between $\mathbf{j}$ and $\mathbf{v}$ is needed. This can be found[33] by using the two-fluid model. The quasiparticle excitation spectrum, $E(\epsilon) = (\epsilon^2 + |\Delta(s)|^2)^{1/2}$, is modified by a Doppler shift to $E(\epsilon) + \mathbf{v}_f \cdot \mathbf{v}$. Here ϵ is the quasiparticle energy referred to the Fermi surface, $\Delta(s)$ denotes the OP dependence on the point s on the Fermi surface[34], and $\mathbf{v}_f$ is the Fermi velocity. This leads to a relation between $\mathbf{j}$ and $\mathbf{v}$ of the form

$$\mathbf{j}(\mathbf{v}) = \mathbf{j}_{lin}(\mathbf{v}) + \mathbf{j}_{nl}(\mathbf{v}). \tag{2.3}$$

After some algebra[24,27], the linear and nonlinear parts can be written, respectively, as:

$$\mathbf{j}_{lin}(\mathbf{v}) = -eN_f \int_{FS} d^2s \, n(s)\mathbf{v}_f(\mathbf{v}_f \cdot \mathbf{v}), \tag{2.4a}$$

$$\mathbf{j}_{nl}(\mathbf{v}) = -2eN_f \int_{FS} d^2s \, n(s)\mathbf{v}_f \int_0^\infty d\epsilon \, f(E(\epsilon) + \mathbf{v}_f \cdot \mathbf{v}), \tag{2.4b}$$

where N_f is the total density of states at the Fermi level, $n(s)$ the local density of states at the Fermi surface (FS), normalized to unity, and f the Fermi function. The first term in (2.3), given by (2.4a), is the usual linear relation $\mathbf{j}_{lin} = -e\tilde{\rho}\mathbf{v}$, where $\tilde{\rho}$ is the superfluid density tensor. At $T = 0$ the nonlinear (in $\mathbf{v}$) corrections, described by (2.4b), can be written as:

$$\mathbf{j}_{nl}(\mathbf{v}) = -2eN_f \int_{FS} d^2s\, n(s)\mathbf{v}_f \Theta(-\mathbf{v}_f \cdot \mathbf{v} - |\Delta(s)|)[(\mathbf{v}_f \cdot \mathbf{v})^2 - |\Delta(s)|^2]^{1/2}, \tag{2.5}$$

which is valid for any $\Delta(s)$. The key point is that the step function in Eq.(2.5) restricts the integration over the FS by

$$|\Delta(s)| + \mathbf{v}_f \cdot \mathbf{v} < 0. \tag{2.6}$$

Thus, when the OP has nodes (or very deep minima) in the Fermi surface, only regions near these nodes participate in populating the quasiparticle spectrum. The integration is dominated by contributions from these regions, and can be written as[28] a sum over local contributions from each of them. The values of the Fermi velocity in the integrand can be replaced by their *local* values at the corresponding nodal region. We need, therefore, more information on the geometry of the superconductor and the angular dependence of the order parameter to carry out the above integration.

B. Geometry and order parameters

We will consider superconducting materials of orthorhombic or higher symmetry and denote the crystallographic axes as a, b and c, corresponding as customary to the x, y and z directions. We will assume that the samples are infinite in a plane parallel to the direction of the applied field, and of thickness d in the direction normal to this plane. This allows us to solve (2.2) and (2.3) analytically. Effects of the sample finite extension in the plane would have to be taken into account numerically, but this is unnecessary since it has been shown in the context of d-wave pairing[35], that such effects merely lead to a small increase in the amplitude of the nonlinear signal, and to no change in its angular or field dependence. On the other hand, the effects of the thickness d are very important and we will include them fully.

We will consider two simple types of p-wave OP's in this paper. The first is representative of the case where the OP has point nodes, as might occur[3,4,6] in Sr_2RuO_4. Up to a phase factor (the nonlinear electrodynamic effects depend only on the absolute value of the OP) we write for the angular dependence of the OP near the nodes:

$$\Delta(\theta) = \Delta_0 \sin(\theta), \tag{2.7}$$

where θ is a polar angle. Only the local properties at the nodes are important: the form (2.7) is assumed only near the nodes, e.g. near $\theta = 0$ it means $\Delta(\theta) \approx \Delta_0\theta$. Thus, the parameter Δ_0 must be thought of as the slope of the OP near the node, rather than its maximum value. The second type we will consider is a prototype of OP's with line nodes, as they might occur in some heavy fermion compounds[11] or even in[22] Sr_2RuO_4. Again, up to an unimportant phase factor, we assume the form for the angular dependence near the nodal line:

$$\Delta(\theta) = \Delta_0 \cos(\theta), \tag{2.8}$$

where the above warning as to the interpretation of Δ_0 as the slope near the nodal region must be repeated. These two forms are archetypes for the possibly more intricate forms of the angular dependence of the OP in real materials. In non s-wave superconductors, the OP need not belong to a one-dimensional representation. Because of this, there may be OP collective modes[7,36] and internal structure effects that are not included in our considerations. The angular dependence of the OP, however, will be in a solid very strongly pinned[7] by crystal effects (this is obviously not the case in liquid ^{3}He). The internal structure of the OP should then not affect our nonlinear results, since only the application of small dc fields is involved.

The experimental setup we envision would involve applying a field parallel to the $a-c$ plane, with the direction normal to the slab being along the b axis[37]. The sample would then be rotated about the b axis while the magnetic field remains fixed. The currents then flow in various directions depending on their orientation relative to the OP under consideration. We will denote by ψ the angle between the applied field $\mathbf{H}_a$ and the z axis and we will investigate the angular dependence of the transverse magnetic moment or the torque as a function of ψ. We will also calculate the field dependence of the penetration depth for the directions of symmetry.

In this geometry we can solve the problem analytically. When $\mathbf{H}_a$ is applied in the $a-c$ plane, the fields have only x and z components, which depend *only* on the coordinate y. Eq. (2.2) then reduces to

$$\frac{d^2\mathbf{v}}{dy^2} + \frac{4\pi e}{c^2}\mathbf{j}(\mathbf{v}) = 0. \tag{2.9}$$

For our given geometry, j_{nli} and v_i have odd parity with respect to the y coordinate, so it is sufficient to solve the boundary value problem for $y \geq 0$. The two required boundary conditions are:

$$\frac{c}{e}\left.(\nabla\times\mathbf{v})\right|_{y=d/2}=\mathbf{H}_a, \tag{2.10a}$$

$$\left.\mathbf{v}\right|_{y=0}=0. \tag{2.10b}$$

We can now proceed to explicitly calculating the nonlinear currents.

C. Nonlinear currents

First, we carry out the integration in Eq. (2.5). This can be performed exactly on a three dimensional Fermi surface, without the need to take recourse to the approximations discussed in Appendix A of Ref. 27. The relevant regions of integration as discussed below (2.6) are contained within a small range near the nodes, with boundaries that can be expressed in terms of limiting angles θ_c, as determined from $(\mathbf{v}_f\cdot\mathbf{v})^2=|\Delta(\theta_c)|^2$.

Consider first the OP given in Eq.(2.7). In this case $\mathbf{v}_f(s)$ can be replaced in the relevant regions of the integrand by its local value, along the z axis, at the nodes. By symmetry, we can restrict ourselves to the node at $\theta=0$ since the contribution from $\theta=\pi$ is identical. Thus, we have $\mathbf{v}_f\approx(0,0,v_{fz})$, and the restriction (2.6) means that in performing the integral in (2.5), we can replace $\int_{FS}d^2s\,n(s)$ by $\int_{\Omega_c}d\phi\theta d\theta/4\pi$, where Ω_c denotes the region $|\theta|<\theta_c$, with $\theta_c^2=(v_{fz}v_z)^2/\Delta_0^2$, and with no restrictions on ϕ. It is easy to see that this yields only a z-component to the nonlinear current. The integrals are elementary and one finds:

$$j_{nlz}=\frac{1}{3}eN_f\frac{v_{fz}^4}{\Delta_0^2}v_z^3, \tag{2.11}$$

where Δ_0 the local gap slope.

For the case of an order parameter as given in (2.8), where the nodal line is at $\theta=\pi/2$, we can take $v_{fz}=0$ over the region of integration. which is then limited to $|\theta-\pi/2|<\theta_c$, where $(\theta_c-\pi/2)^2=(\cos\alpha v_f v_\perp/\Delta_0)^2$. Here $v_\perp$ is the projection of $\mathbf{v}$ on the $x-y$ plane, and α the angle between $v_\perp$ and the in-plane v_f. We make the replacement $\int_{FS}d^2s\,n(s)\rightarrow\int_{\Omega_c}d\phi d\theta/4\pi$, where Ω_c is the region of integration as defined by θ_c. For orthorhombic symmetry, v_f depends on ϕ. We then transform the integral over ϕ to one over α using the relation $\phi=\beta+\alpha$, where β is the (fixed) angle $v_\perp$ makes with the x axis, and α is restricted (from Eq. (2.6)) to $\pi/2<\alpha<3\pi/2$. The integration is lengthier but straightforward and results in two components to the current. The x component is:

$$j_{nlx}=\frac{1}{3}eN_f\frac{v_{fx}^3}{\Delta_0}v_x\left(v_x^2+v_y^2\right)^{1/2}\Lambda_x(\mathbf{v}), \tag{2.12}$$

where $\Lambda_x(\mathbf{v})\equiv(1/5)[(3+2\delta^2)+(1-\delta^2)(v_x^2/(v_x^2+v_y^2))]$ ($\Lambda_x\equiv1$ when the material has tetragonal symmetry), v_{fx} is the Fermi speed along the x axis and the $a-b$ plane anisotropy is characterized by $\delta\equiv\lambda_x/\lambda_y$, where λ_i denotes the penetration depth along the i direction. The y component, j_{nly}, is obtained by making the obvious replacements in (2.12). The coefficients in (2.11) and (2.12) are given in terms of the local values of the Fermi velocity and are therefore independent of the detailed shape of the Fermi surface.

These expressions for $\mathbf{j}$ as a function of $\mathbf{v}$ can be inserted into Eq. (2.9), which then becomes a nonlinear differential equation in terms of the flow field only. Implementing a perturbation scheme to lowest order in the flow field will allow exact expressions for both OP's to be obtained. This is addressed in the next subsection.

D. Perturbation solution

For an OP of the form (2.7), we can insert Eq. (2.11) into Eq. (2.9). We can then write the equation for the component carrying the nonlinear term as:

$$\frac{\partial^2 v_z}{\partial Y_z^2}-v_z+\left(\frac{v_z}{v_{cz}}\right)^2v_z=0, \tag{2.13}$$

where we have introduced the dimensionless coordinate $Y_i\equiv y/\lambda_i$. The local critical velocity is defined as $v_{ci}\equiv\Delta_0/v_{fi}$, (for $i=x,y,z$) and we have used the three dimensional relation $1/\lambda_i^2=(4\pi e^2/3c^2)N_f v_{fi}^2$. From Eq. (2.10a), the boundary condition at the surface $Y_i=Y_{is}\equiv d/(2\lambda_i)$ can be written in terms of our new variables:

$$\left.\frac{\partial v_x}{\partial Y_x}\right|_{Y=Y_{xs}}=-\frac{e\lambda_x}{c}H_a\cos\psi,\qquad\left.\frac{\partial v_z}{\partial Y_z}\right|_{Y_z=Y_{zs}}=\frac{e\lambda_z}{c}H_a\sin\psi. \tag{2.14}$$

We now expand $v_z(Y_z)$ to first order in the parameter $\alpha_z = (v_{fz}/\Delta_0)^2$, which is small in the typical experimental situations. We write $v_z(Y_z) = v_{0z}(Y_z) + \alpha_z\, v_{1z}(Y_z)$. To zeroth order, we have the usual linear equation:

$$\frac{\partial^2 v_{0z}}{\partial Y_z^2} - v_{0z} = 0, \tag{2.15}$$

with v_{0z} satisfying the boundary conditions (2.14), (2.10a). The solution is:

$$v_{0z}(Y_z) = c_z \sinh(Y_z), \tag{2.16}$$

where

$$c_z = \frac{e\lambda_z H_a \sin\psi}{c\cosh(Y_{zs})}. \tag{2.17}$$

The nonlinear part v_{1z} satisfies:

$$\frac{\partial^2 v_{1z}}{\partial Y_z^2} - v_{1z} + v_{0z}^3 = 0. \tag{2.18}$$

The boundary conditions are $\partial v_{1z}/\partial Y_z|_{Y=Y_{zs}} = 0$ and $v_{1z}(0) = 0$. The complete solution to Eq. (2.18) is found by elementary methods and is given by:

$$v_{1z}(Y_z) = (1/8)c_z^3\left[c_1 \sinh(Y_z) + 3Y_z\cosh(Y_z) - (1/4)\sinh(3Y_z)\right], \tag{2.19}$$

where $c_1 = (3/2)(\sinh(2Y_{zs}) - 2Y_{zs})\tanh(Y_{zs}) - 9/4$.

The magnetic field in the sample can be calculated from the field $\mathbf{v}$ via Eq. (2.1). Including also the purely linear component arising from v_x we obtain:

$$H_x(Y_z) = \frac{H_a\sin\psi}{\cosh(Y_{zs})}\left[\cosh(Y_z) + \frac{1}{8}\left(\frac{H_a\sin\psi}{H_{0z}\cosh(Y_{zs})}\right)^2 f_H(Y_z)\right], \tag{2.20a}$$

$$H_z(Y_x) = \frac{H_a\cos\psi}{\cosh(Y_{xs})}\cosh(Y_x), \tag{2.20b}$$

where the nonlinear depth dependence is contained in f_H:

$$f_H(Y_z) = 3Y_z\sinh(Y_z) - (3/4)\cosh(3Y_z) + (c_1+3)\cosh(Y_z), \tag{2.20c}$$

and we have introduced the characteristic field

$$H_{0i} = \frac{\phi_0}{\pi^2\lambda_i\xi_i}. \tag{2.21}$$

Here ϕ_0 is the superconducting flux quantum, and $\xi_i = v_{fi}/(\pi\Delta_0)$ is the local coherence length. As opposed to the d-wave case where the nodal lines give rise to a quadratic nonlinear contribution, we now find a nonlinear effect cubic in the applied field. Physically, this is quite transparent: the phase space volume available to the quasiparticle excitations increases as the cube of the field for point nodes, and as the square for line nodes. The nonlinear term anisotropically increases the magnetic field penetration because of quasiparticle occupation near the nodes, i.e., fewer Cooper pairs are participating in the current responsible for bulk flux exclusion.

We can gain some insight into these results by examining the spatial dependence of the nonlinear part of the field as displayed in Fig. 1. There the quantity H_{nlx}, defined as the last term in (2.20a) normalized to unity at its maximum, is plotted as a function of dimensionless distance D from the surface ($D = Y_{sz} - Y_z$). The thickness of the sample is taken to be $d >> \lambda_z$ so that the behavior shown is that corresponding to a thick slab. The nonlinear field is constrained by the boundary conditions to vanish at the surface: the boundary condition implies an extremum for the nonlinear flow field at the surface and since $H_x \propto \partial v_{1z}/\partial Y_z$, we see that H_{nlx} must vanish there. It then increases rapidly reaching its maximum at about one half of a penetration depth and then decays exponentially inside the sample, as does the linear part. Thus arises the characteristic maximum of the nonlinear field seen in this Figure.

The current is most easily obtained from $\mathbf{H}$ through Ampère's law for steady-state currents, which gives the result:

$$j_z(Y_z) = -\frac{cH_a \sin\psi}{4\pi\lambda_z \cosh(Y_{zs})} \left[\sinh(Y_z) - \frac{1}{8} \left(\frac{H_a \sin\psi}{H_{0z} \cosh(Y_{zs})} \right)^2 f_J(Y_z) \right], \tag{2.22a}$$

$$j_x(Y_x) = \frac{cH_a \cos\psi}{4\pi\lambda_x \cosh(Y_{xs})} \sinh(Y_x). \tag{2.22b}$$

The Y_z dependence of the nonlinear current is contained in $f_J(Y_z)$ which is given by:

$$f_J(Y_z) = -3Y_z \cosh(Y_z) + (9/4)\sinh(3Y_z) - (c_1 + 6)\sinh(Y_z). \tag{2.22c}$$

In Eq. (2.22a), the first term on the right is the linear contribution, proportional to the applied field, while the second term is the nonlinear correction, modifying the total current.

We now turn to the case where the OP is of the form (2.8). For simplicity, we consider tetragonal symmetry and quote the results for the orthorhombic case later. The current in Eq. (2.12) can be simplified using that the magnetic field is applied in the $x - z$ plane, so that v_y is zero. The current is substituted in (2.9) to give, for the component containing the nonlinear term:

$$\frac{\partial^2 v_x}{\partial Y_x^2} - v_x + \frac{|v_x|}{v_{cx}} v_x = 0. \tag{2.23}$$

The method of solution is identical to that above with the only major difference being that the expansion parameter is now $\alpha_x = (v_{fx}/\Delta_0)$, linear rather than quadratic. The linear velocity field v_{0x} is $v_{0x} = -c_x \sinh(Y)$, while the nonlinear term is written as

$$v_{1x}(Y_x) = (1/6)c_x|c_x| \left[\cosh(2Y_x) - 4\cosh(Y_x) + 4c_2 \sinh(Y_x) + 3\right], \tag{2.24}$$

where

$$c_x = \frac{e\lambda_x H_a \cos\psi}{c \cosh(Y_{xs})}, \qquad c_2 = \tanh(Y_{xs}) - \sinh(Y_{xs}). \tag{2.25}$$

The magnetic field is calculated again via the London equation. In this case the nonlinear part is (as in the d-wave case) proportional to H_a^2, rather than to H_a^3 as was found for the point nodes. This follows again from phase-space arguments. After including the contribution from the purely linear component of $\mathbf{v}$ one finds:

$$H_z(Y_x) = \frac{H_a \cos\psi}{\cosh(Y_{xs})} \left[\cosh(Y_x) + \frac{1}{6} \left(\frac{H_a |\cos\psi|}{H_{0x} \cosh(Y_{xs})} \right) g_H(Y_x) \right], \tag{2.26a}$$

$$H_x(Y_z) = \frac{H_a \sin\psi}{\cosh(Y_{zs})} \cosh(Y_z). \tag{2.26b}$$

Here g_H, which determines the nonlinear contribution to the magnetic field penetration, is given by:

$$g_H(Y_x) = -2\sinh(2Y_x) + 4\sinh(Y_x) - 4c_2 \cosh(Y_x). \tag{2.26c}$$

It is again useful to plot the nonlinear component of the magnetic field. We consider H_{nlz}, the last term in (2.26a) normalized to its maximum value. Fig. 2 shows H_{nlz} plotted versus dimensionless distance D from the surface ($D \equiv Y_{sx} - Y_x$). One sees again the rapid increase of the field near the surface of the sample, followed by the usual exponential decay. The plot is very similar to that in Fig. 1 for point nodes, but the field decays less rapidly into the sample. Within about three penetration depths, the nonlinear field is reduced to 20% of its maximum magnitude.

The total current is composed of linear and nonlinear terms, as found from Ampère's law:

$$j_x(Y_x) = \frac{cH_a \cos\psi}{4\pi\lambda_x \cosh(Y_{xs})} \left[\sinh(Y_x) - \frac{1}{6} \left(\frac{H_a |\cos\psi|}{H_{0x} \cosh(Y_{xs})} \right) g_J(Y_x) \right], \tag{2.27a}$$

$$j_z(Y_z) = -\frac{cH_a \sin\psi}{4\pi\lambda_z \cosh(Y_{zs})} \sinh(Y_z). \tag{2.27b}$$

where

$$g_J(Y_x) = 4[\cosh(2Y_x) - \cosh(Y_x) + c_2 \sinh(Y_x)], \tag{2.28}$$

is the function determining the penetration of the nonlinear currents.

We can now use our solutions for both OP's to derive expressions for the experimentally relevant quantities.

E. The transverse magnetic moment

The expression for the magnetic moment in terms of the currents is:[38]

$$\mathbf{m} = \frac{1}{2c}\int d\mathbf{r}\mathbf{r}\times\mathbf{j}(\mathbf{v}). \tag{2.29}$$

By making use of standard identities and the parity of $\mathbf{v}$, Eq. (2.29) can be rewritten[28,39] more conveniently as:

$$m_{x,z} = -\frac{VH_{a\,x,z}}{4\pi} \mp \left.\frac{Ac\,v_{z,x}}{2\pi e}\right|_{y=\frac{d}{2}}, \tag{2.30}$$

where A is the surface area of the plane along which the field is applied, V is the volume of the sample, and we have used that $\mathbf{v}$ is odd in z. The magnetic moment perpendicular to the applied field is given by $m_x\cos\psi - m_z\sin\psi$. The linear terms of the velocity fields contribute to this quantity only if there is anisotropy in the penetration depth tensor. In that case, the linear term in the transverse magnetic moment, denoted by $\tilde{m}_\perp$, is:

$$\tilde{m}_\perp = \frac{1}{4\pi}AH_a(\lambda_z-\lambda_x)\sin 2\psi. \tag{2.31}$$

This term can be distinguished from the nonlinear contribution, $m_\perp$, because of its different field and angular dependences.

For an OP with point nodes, (2.7), $m_\perp$ is obtained from (2.30), (2.19) and (2.20) as:

$$m_\perp(\psi) = \frac{1}{4\pi}A\lambda_z H_a\left(\frac{H_a}{H_{0z}}\right)^2[(3^{3/2}/32)f_s(\psi)]\mathcal{K}_{\mathcal{S}}(Y_{zs}). \tag{2.32}$$

This quantity is proportional to the cube of the applied field, rather than, as in the d-wave case,[24,25,27,28] to the square. This reflects the reduced phase space when the nodal regions are points rather than lines on the FS. Thus larger values of H_a are very advantegeous provided that H_a is kept below the field of first flux penetration, H_{f1}, so that the sample remains in the Meissner regime. The angular dependence of $m_\perp(\psi)$ is contained in $f_s(\psi)$ which is normalized to unity at its maximum and given by:

$$f_s(\psi) = (16/3^{3/2})\cos\psi\sin^3\psi, \tag{2.33}$$

while the dependence of $m_\perp$ on the material thickness d is given by the function $\mathcal{K}_{\mathcal{S}}$,

$$\mathcal{K}_{\mathcal{S}}(Y_{zs}) = (1/2)\mathrm{sech}^4(Y_{zs})\left[3Y_{zs} - 2\sinh(2Y_{zs}) + (1/4)\sinh(4Y_{zs})\right]. \tag{2.34}$$

The torque associated with $m_\perp$ is simply obtained by multiplying (2.32) by H_a, therefore it has the same thickness and angular dependence.

The function $f_s(\psi)$ is displayed as the solid line in Fig. 3. The transverse magnetic moment and torque in this case are maximal for the field direction corresponding to $\psi = \pi/3$, and vanish at directions corresponding to the nodes or antinodes of the OP. The π periodicity of $m_\perp$ matches that of the energy since the angular dependence of the quasiparticle energy arises solely from that of $|\Delta(\theta)|^2$.

Since $m_\perp$ is an extensive quantity and it is often the case that larger samples can be made in film form rather than grown as free standing crystals, it is of considerable interest to examine the thickness dependence of the results, as given by $\mathcal{K}_{\mathcal{S}}$. The behavior of $\mathcal{K}_{\mathcal{S}}$ is displayed in Fig. 4, where $\mathcal{K}_{\mathcal{S}}$ is plotted (solid line) as a function of $Y_{sz}\equiv d/(2\lambda_z)$. It is seen that $\mathcal{K}_{\mathcal{S}}$ increases rapidly with Y_{sz}, reaching 90% of its maximum value of unity when $d\simeq 5\lambda$. If the sample is a thick slab, $d\gg\lambda_z$, then $\mathcal{K}_{\mathcal{S}}\to 1$, so that $m_\perp$ is (for the same area A) maximal and independent of d. On the other hand, the decrease of $\mathcal{K}_{\mathcal{S}}$ with thickness is substantial: for films where $d=\lambda_z$, $\mathcal{K}_{\mathcal{S}}$ is $\mathcal{K}_{\mathcal{S}}(1/2) = .017$, a reduction of over 80%. Such a decrease, however, may very well be compensated by a larger increase in A, compared to a free standing crystal. However, for extremely thin films, $d\ll\lambda_z$, then $\mathcal{K}_{\mathcal{S}}\simeq 1/40(d/\lambda_z)^5$, and despite the increase of H_{f1} in thin films, the amplitude of the signal would almost certainly be too small[40].

When the order parameter is of the form (2.8), the results obtained from the previous expressions (2.24) and (2.26) for a compound with tetragonal symmetry yield, when substituted in (2.30), the expression:

$$m_\perp(\psi) = \frac{1}{4\pi}A\lambda_x H_a\left(\frac{H_a}{H_{0x}}\right)[(4/3^{5/2})f_c(\psi)]\mathcal{K}_{\mathcal{C}}(Y_{xs}). \tag{2.35}$$

We have introduced the fuctions $f_c(\psi)$, and $\mathcal{K}_{\mathcal{C}}$ characterizing, respectively, the angular and the thickness dependences of the result. They are given by:

$$f_c(\psi) = (3^{3/2}/2)|\cos\psi|\cos\psi\sin\psi, \tag{2.36a}$$

$$\mathcal{K}_{\mathcal{C}}\,(Y_{xs}) \;= [\mathrm{sech}(Y_{xs})-1]^2\,[1+2\,\mathrm{sech}(Y_{xs})]\,. \tag{2.36b}$$

The nonlinear transverse moment is now proportional to the square of the applied field, as in the d-wave case, because of the linear character of the nodal regions. The function $f_c(\psi)$ is normalized to unity and it is plotted as the dashed line of Fig. 3. It is seen there that the angular signature is different from that in the previous case: $m_\perp$ has now a maximum when $\psi = \arctan(\sqrt{2}/2)$, although it is zero again for fields applied along the nodes and antinodes ($\psi = \pi/2, 0$) in the OP. As in the previous case, $\mathcal{K}_{\mathcal{C}}$ is small for small thickness. If we are dealing with a thick slab, $\mathcal{K}_{\mathcal{C}} \to 1$, but when $d \sim \lambda_x$, $\mathcal{K}_{\mathcal{C}} \approx .036$. In the limit $d \ll \lambda_x$, $\mathcal{K}_{\mathcal{C}} \simeq 3/64(d/\lambda_x)^4$. As seen in Fig. 4, the overall characteristics of $\mathcal{K}_{\mathcal{C}}$ (dashed line) are very similar to those of $\mathcal{K}_{\mathcal{S}}$, but $\mathcal{K}_{\mathcal{C}}$ is larger in magnitude throughout. Both curves show a 50% drop in signal when $d \simeq 3\lambda_x$.

It is somewhat tedious but straightforward to generalize, starting from the form (2.12), the calculation of the fields and currents for this order parameter to the case where there is penetration depth anisotropy in the $a-b$ plane. The result is that, when the sample is rotated about the b axis, Eq. (2.35) is simply modified to:

$$m_\perp(\psi) = \frac{1}{4\pi}A\lambda_x H_a\left(\frac{H_a}{H_{0x}}\right)[(4/3^{5/2})f_c(\psi)]\mathcal{K}_{\mathcal{C}}(Y_{xs})\Gamma_x, \tag{2.37}$$

where $\Gamma_x \equiv (1/5)(4+\delta^2)$. Thus, the angular, field and thickness dependences remain the same, while only an overall anisotropy factor is needed.

F. Penetration depth

Measuring the field dependence of the penetration depth at low temperatures is another possible way of exploring the nonlinear Meissner effect. The reduction of the current via quasiparticle population results in a lower superfluid density and hence a larger penetration depth. Indeed, this was the first quantity studied[24] in this area, although it is only very recently that experimental measurements[41] have been attempted for HTSC's.

In the presence of nonlinear effects, several possible definitions of the penetration length which coincide in the linear limit give slightly different results. The appropriate definition depends on the experimental setup. We have calculated above the spatial current and field distributions, and these results can be used to obtain the nonlinear contributions to λ for any definition. We briefly illustrate this here by computing the components of the penetration depth along the x and z directions via the definition:

$$\frac{1}{\lambda_z(\mathbf{H}_a)} = \frac{1}{\lambda_z H_a}\left(\frac{\partial H_x}{\partial Y_z}\right)_{Y=Y_{zs}}, \qquad \frac{1}{\lambda_x(\mathbf{H}_a)} = \frac{1}{\lambda_x H_a}\left(\frac{\partial H_z}{\partial Y_x}\right)_{Y=Y_{xs}}, \tag{2.38}$$

where λ_i is the zero field penetration depth along the i direction. We will assume that the field is applied along a symmetry direction for each OP and will not place any restrictions on the thickness d.

We consider first the order parameter with point nodes, (2.7). The penetration depth when the applied field is perpendicular to the z-axis, ($\psi = \pi/2$) is obtained from (2.38) and (2.20):

$$\frac{1}{\lambda_z(H_a)} = \frac{1}{\lambda_z}\left\{\tanh(Y_{zs}) - \frac{3}{32}\left(\frac{H_a}{H_{0z}}\right)^2\mathcal{L}_{\mathcal{S}}\right\}, \tag{2.39}$$

where $\mathcal{L}_{\mathcal{S}} = \mathrm{sech}^4(Y_{zs})[-4Y_{zs} + \sinh(4Y_{zs})]$. The most obvious difference between this and the results for d-wave is that the field correction is proportional to the square of the field, rather than to the field itself. This follows, once more, from phase space arguments. For a thick slab, $\mathcal{L}_{\mathcal{S}} \to 8$, while in the very thin film limit, $\mathcal{L}_{\mathcal{S}} \approx (4/3)(d/\lambda_z)^3$.

For the OP given in (2.8) one similarly gets:

$$\frac{1}{\lambda_x(H_a)} = \frac{1}{\lambda_x}\left\{\tanh(Y_{xs}) - \frac{2}{3}\left(\frac{H_a}{H_{0x}}\right)\mathcal{L}_{\mathcal{C}}\right\}, \tag{2.40}$$

where $\mathcal{L}_{\mathcal{C}} = 1 - \mathrm{sech}^3(Y_{xs})$, which goes to unity for a thick slab. For a very thin film superconductor, $\mathcal{L}_{\mathcal{C}} = 2/3(d/\lambda_x)^2$. Here the penetration depth correction, $\delta\lambda/\lambda_x$ is linear in the applied filed as in the d-wave case, as a result of the presence in both cases of nodal lines. The dependence on thickness in the very thin film limit is cubic in d for the point nodes and quadratic for line nodes.

III. DISCUSSION

We have calculated the magnitude of the nonlinear electrodynamics effects as a function of field and angle. We believe that some remarks are now in order as to the feasibility of observing effects of the rough magnitude of those predicted. In making these remarks, we do not claim any experimental expertise in the relevant areas. We have in mind compounds with materials characteristics such as those of UBe_{13} or Sr_2RuO_4. In mentioning these compounds, we do not intend to propose that any of them belong to a specific pairing state. We merely wish to roughly estimate the level of the signal that would be predicted in the event that the material turned out to have a pairing state with a certain nodal structure. Our considerations can straightforwardly be extended to other materials.

First, our calculations have been performed, strictly speaking, in the low temperature limit. In practice, this means[25,26] the temperature regime in the region $T < \tilde{T}(H) \lesssim \Delta_0 H/H_0$, so that thermal excitations do not destroy[25] the nonlinear Meissner effect. Assuming that, in order to maximize the signal, the applied field is close to H_{f1}, the field of first flux penetration, this still implies that the experiments must be performed at temperatures well below T_c. This means, for the materials of interest, at dilution refrigerator temperatures. This is undeniably a disadvantage when compared with the situation for HTSC's, but one that can be overcome by using torque magnetometry[30] or torsion oscillator[29] techniques to measure the torque associated with the transverse moment. These techniques can be adapted to use in conjunction with a dilution refrigerator and their sensitivity can surpass[31] that of the SQUID methods used for HTSC's[43,44]. These considerations pertain to the transverse moment and the associated torque. Several groups are planning, in the context of checking the very low temperature behavior of λ in HTSC's for deviations from the linear power law behavior, measurements of λ at dilution refrigerator temperatures. These techniques could be combined with the high resolution methods already employed[41] to measure the field dependence of λ.

We consider next the magnitude of the low T effect. The maximum amplitude of the transverse moment depends on the values of the penetration depth, the characteristic field H_{0i}, and the maximum field one can apply while remaining in the Meissner regime, which is H_{f1}. Because $m_\perp$ is an extensive quantity, it also depends on the size (specifically the surface area) of the samples available. As an illustrative exercise, we have estimated a putative signal for the transverse magnetic moment amplitude for a number of compounds by getting from the literature[2,10,44–47] values of available crystal sizes and of the experimental parameters (such as penetration depths, and correlation lengths in the appropriate directions) that appear in our expressions. These values are subject to very considerable uncertainty and in most cases different references do not agree with each other, but they are sufficient for the purposes of our exercise. By inserting them in the appropriate formulae, (2.32), and (2.35), we obtain numerical values of the possible signal. The results are summarized in Table I, where we present our estimate for the maximum amplitude $M_\perp$ for several materials. $M_\perp$ is defined as the value of $m_\perp$ for a thick slab at $H_a = H_{c1}$ and at the angle ψ for which $m_\perp$ is maximal. The critical field H_{c1} is calculated from[48] $H_{c1} = (\phi_0/(4\pi\lambda^2))\ln(\lambda/\xi)$ and is used as a conservative approximation to H_{f1} since H_{c1} is smaller (by a large factor[49] for YBCO) than H_{f1}. We have also included in the Table, for the purposes of comparison, one typical HTSC compound (YBCO), with the signal in that case computed from Ref. 28 for a d-wave state. For the other materials, we have assumed the OP in Eq. (2.7) for Sr_2RuO_4, while for the listed heavy fermion materials and organic salt we have taken the OP of Eq. (2.8). It bears repeating that these choices are illustrative and do not imply any judgement on our part as to the likelihood of what the pairing state actually might be. Rather, our point is that the techniques in this paper can be implemented to infer the nodal structure of the pairing state. The results in Table I are expressed in physical units and also, for purposes of comparison, as ratios to the corresponding estimate for YBCO in a d-wave state. The numbers in the table are very encouraging: they are in all cases comparable to or larger than those for YBCO and always comfortably exceed the resolution of the experimental techniques discussed above.[29,30] For the penetration depth results, the situation is similarly favorable, since the changes in the penetration depth induced by a field close to H_{f1} are considerably larger than the lower limit (a few Å resolution) already achieved[41] in YBCO.

We have to consider also the limitations of this work and the presence of other phenomena, besides temperature excitations, that may reduce the signal. First, there is the question of impurities. As has been seen in the context of YBCO,[25,26] good quality samples characterized by a transition temperature not appreciably degraded, and by the appropriate power law behavior of λ with temperature, should exhibit a signal substantially of the magnitude calculated here for a clean system. The decrease in the nonlinear signal associated with nonlocal effects at lower fields can also complicate the situation[50]. However, these effects are quite small for fields close to H_{f1} in the typical situation where this field[49] is considerably larger than the equilibrium H_{c1}. In any case nonlocal effects are absent for several special crystal orientations[51,52], which can then be chosen. There also important questions as to what the effect of using more realistic forms (still containing point or line nodes) of the order parameter would be, or of including in more detail the local value properties of the Fermi surface. All told, however, we believe that the estimates in the Table show that there is a sufficient cushion between the maximum value and the experimental resolution so that one can expect an observable signal.

In conclusion, we have calculated here the nonlinear signal arising from the presence of point or line nodes in some simple p-wave order parameters. We have shown that there is a likelihood that these effects will be observable in materials currently being studied. The results given can straightforwardly be extended, if and when the experimental situation warrants it, to the study of the low frequency response[53], to more complicated or mixed order parameters, and a more general node spectroscopy procedure for p-wave materials can be performed as in Ref. 28.

ACKNOWLEDGMENTS

We are indebted to Igor Žutić for conversations on the theories presented in this paper and for reading a draft of the manuscript. We thank Paul Crowell and Allen Goldman for numerous conversations concerning what can and cannot be done experimentally. This work was supported in part by the Petroleum Research Fund, administered by the ACS.

---

[*] Electronic address: khalter@physics.spa.umn.edu

[+] Electronic address: otvalls@tc.umn.edu

[1] J.F. Annett, N. Goldenfeld and A.J. Leggett, in *Physical properties of high temperature superconductors V*, D.M. Ginzburg, ed., World Scientific, Singapore (1996).

[2] T.M. Riseman *et al.*, Nature **396**, 242 (1998).

[3] K. Ishida *et al.*, Nature **396**, 658 (1998).

[4] M. Matsumoto and M. Sigrist, cond-mat/9903004.

[5] G.M. Luke *et al.*, Nature **394**, 558 (1998).

[6] M. Sigrist *et al.*, cond-mat/9902214.

[7] H. Kee, Y. Kim, K. Maki, cond-mat/9907276.

[8] M. Rice, Nature **396**, 627 (1998).

[9] A.J. Leggett, Rev. Mod. Phys. **47**, 331 (1975).

[10] A. Amato, Rev. Mod. Phys. **69**, 1119 (1997).

[11] K. Machida, T. Nishira, and T. Ohmi, cond-mat/9906105.

[12] R. Lal and S.K. Joshi, Phys. Rev. **41**, 1894, (1990).

[13] K. Kanoda *et al.* Phys. Rev. **B54**, 76, (1996).

[14] L.P. Le *et al.*, Phys. Rev. Lett. **68**, 1923 (1992).

[15] A. G. Lebed, Phys. Rev. Lett. **59**, R721 (1999)

[16] K. Kanoda, K. Akiba, K. Suzuki, and T. Takahashi, Phys. Rev. Lett. **65**, 1271 (1990)

[17] D. Achkir, Phys. Rev. B **47**, 11595 (1993).

[18] S. Belin, K. Behnia, Phys. Rev. Lett. **79**, 2125 (1997).

[19] H. Mayaffre *et al.* Phys. Rev. Lett. **75**, 4122, (1995).

[20] M. Miyazaki *et al* cond-mat/9908488.

[21] M. Lang *et al*,Phys. Rev. Lett. **69**, 1443 (1992).

[22] Y. Hasegawa, K. Machida, and M. Ozaki, cond-mat/9909316.

[23] S.R. Bahcall, Phys. Rev. **76**, 3634, (1996).

[24] S.K. Yip and J.A. Sauls, Phys. Rev. Lett. **69**, 2264 (1992).

[25] B.P. Stojković and O.T. Valls, Phys. Rev. **B51**, 6049, (1995).

[26] D. Xu, S.K. Yip and J.A. Sauls, Phys. Rev. **B51**, 16233, (1995).

[27] I. Žutić and O.T. Valls, Phys. Rev. **B54**, 15500, (1996).

[28] I. Žutić and O.T. Valls, Phys. Rev. **B56**, 11279, (1997).

[29] P.A. Crowell *et al.*, Rev. Sci. Inst. **67**, 4161, (1996).

[30] C. Rossel *et al.*, J. Appl. Phys. **79**, 8166 (1996).

[31] A.M. Goldman, private communication.

[32] As explained below, any contributions associated with internal degrees of freedom of the OP should be unimportant in solid systems at small applied fields.

[33] J. Bardeen, Phys. Rev. Lett. **1**, 399 (1958).

[34] Possible contributions arising from finite spin of the Cooper pairs are negligible compared to the diamagnetic terms.

[35] I. Žutić and O.T. Valls, J. Comp. Phys. **136**, 337 (1997).

[36] L. Tewordt, Phys. Rev. Lett. **83**, 1007 (1999).

[37] For any situation where the crystallographic direction of the point nodes, or the plane of the line nodes, is different from that assumed here, our considerations and results apply after performing the appropriate change of labels.
[38] J.D. Jackson, *Classical Electrodynamics* (Wiley, New York, 1975), p.181.
[39] See E.H. Brandt, Phys. Rev. Let. **76**, 4030 (1994); **71**, 2821 (1993)
[40] In addition, for very thin films ($d \lesssim \xi$) problems associated with Andreev bound states may occur: see H. Walter *et al.* Phys. Rev. Lett. **80**, 3598 (1998).
[41] C. Bidinosti and W. Hardy, cond-mat/9808231 (to appear in Phys. Rev. Lett.).
[42] P. Crowell, private communication.
[43] J. Buan *et al.*, Phys. Rev. **72**, 2632 (1994).
[44] A. Bhattacharya *et al.*, Phys. Rev. Lett. **82**, 3132, (1999).
[45] G.M. Luke *et al.* Phys. Lett. **A157**, 173, (1991).
[46] P.A. Mansky, G. Danner, and P.M. Chaikin, Phys. Rev. B **52**, 7554, (1995).
[47] R. N. Kleinman *et al*, Phys. Rev. Lett. **69**, 3120, (1992).
[48] P.G. de Gennes, *Superconductivity of Metals and Alloys* (W.A. Benjamin, Inc., New York, 1966), p. 66.
[49] A.Bhattacharya *et al.*, Phys. Rev. Lett. **83**, 887 (1999).
[50] M.R. Li *et al.*, Phys. Rev. Lett. **81**, 5640 (1998).
[51] I. Kostzin and A. J. Leggett, Phys. Rev. Lett. **79**, 135 (1997).
[52] M.R. Li *et al*, cond-mat/9907189.
[53] I. Žutić and O.T. Valls, Phys. Rev. **B58**, 8738, (1998).

FIG. 1. Spatial behavior of the nonlinear field when the OP has point nodes. The quantity ploted is H_{nlx}, as given by the last term in (2.20a), normalized to unity at its maximum. This quantity is plotted as a function of D, the distance from the surface in units of λ_z: $D \equiv Y_{sz} - Y_z$. The sample has thickness $d >> \lambda_z$. The nonlinear field increases rapidly until the distance from the surface is about half λ_z and then decreases exponentially, as in the usual linear case.

FIG. 2. The nonlinear z component of the magnetic field for a material with an OP of the form (2.8). The quantity plotted is H_{nlz}, the last term in (2.26a), normalized to unity at its maximum. It is plotted versus dimensionless distance from the surface: $D \equiv Y_{sx} - Y_x$. The material thickness is $d >> \lambda_x$. The behavior is qualitatively similar to that shown in the previous Figure, but the maximum occurs at a somewhat greater depth.

FIG. 3. The angular dependence of the normalized transverse magnetic moment is plotted versus ψ (the angle between $\mathbf{H}_a$ and the z axis, in radians). The solid line is the function $f_S(\psi)$ given in (2.33) for an OP of the form (2.7), while the dashed line is $f_C(\psi)$ from (2.36) for the OP (2.8). Both functions are normalized to their maximum values. Their maxima are at $\psi = \pi/3$ and $\psi = \arctan(\sqrt{2}/2)$ respectively and their periodicity is π.

FIG. 4. The symbol K stands for the functions $\mathcal{K}_\mathcal{S}$ (solid curve) and $\mathcal{K}_\mathcal{C}$ (dashed curve), which characterize the thickness dependence of $m_\perp$. They are plotted versus the dimensionless thickness Y_s (Y_s represents $d/2\lambda_z$ for $\mathcal{K}_\mathcal{S}$ and $d/2\lambda_x$ for the $\mathcal{K}_\mathcal{C}$ plot.) The exponential increase of the functions towards unity is rapid and the corresponding bulk regime arises when the material thickness d is about five penetration depths.

TABLE I. Illustrative estimates of possible nonlinear signal for various materials of uncertain OP nodal structure. Values for d-wave YBCO are also given for comparison purposes. The magnetic field is in Gauss, and the maximum transverse magnetization amplitude, $M_\perp$, as defined in the text, is given in ($\times 10^{-8}$) emu's. The quantities λ and H_0 are for the relevant directions (see text).

Compound	Area (mm^2)	λ (Å)	H_0	$\frac{H_{c1}}{H_0}$	$M_\perp$	$\frac{M_\perp}{M_\perp(YBCO)}$
YBCO	1.8	1400	7607	.048	2.1	1
UBe_{13}	5	11000	204	.032	2.4	1.1
UPt_3	150	15000	71	.045	66	31.4
Sr_2RuO_4	25	1940	147	.29	22.5	10.7
$(TMTSF)_2ClO_4$	1	5000	43	.25	2.7	1.3

Figure 1 Halterman and Valls

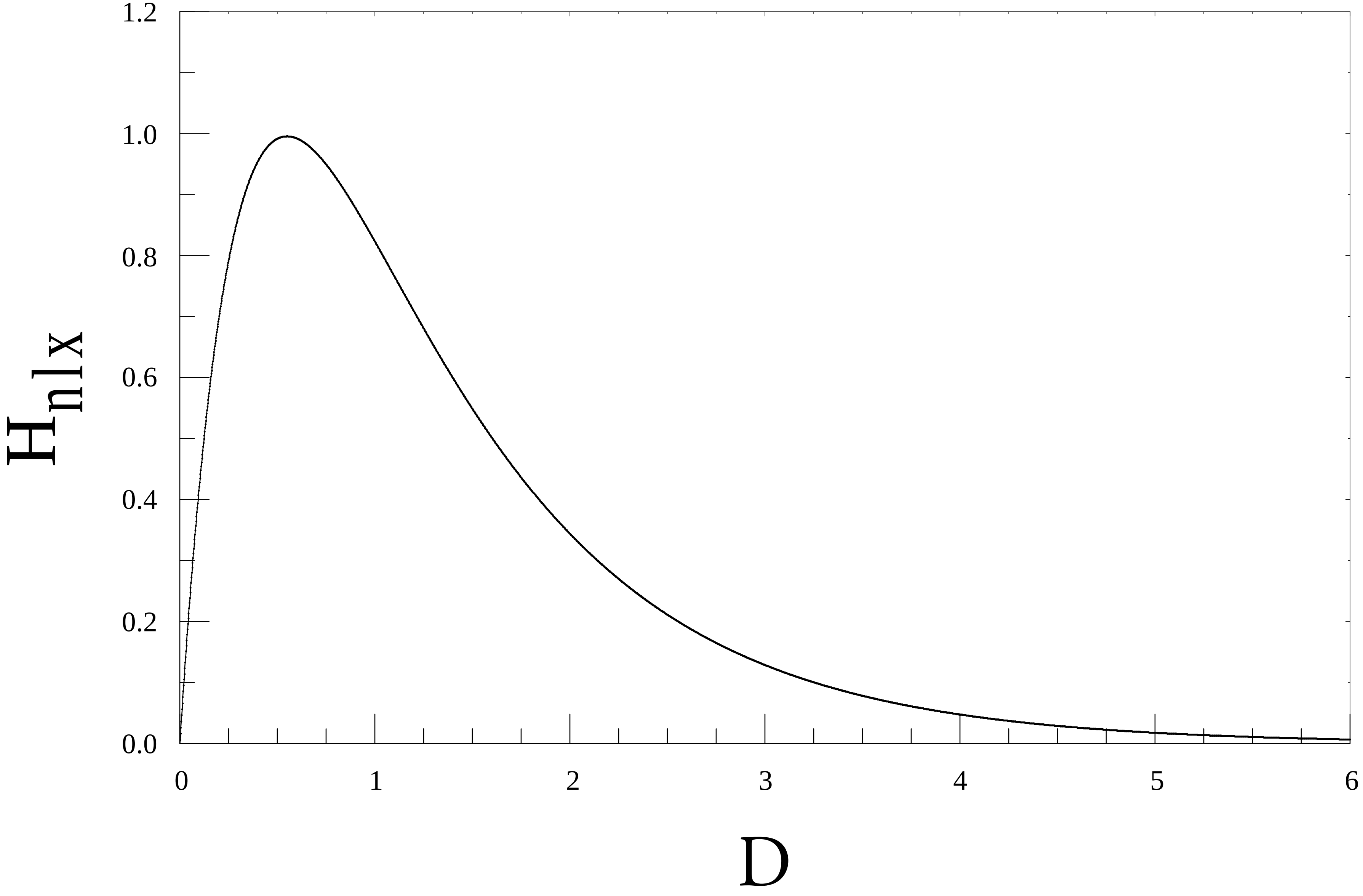

Figure 2   Halterman and Valls

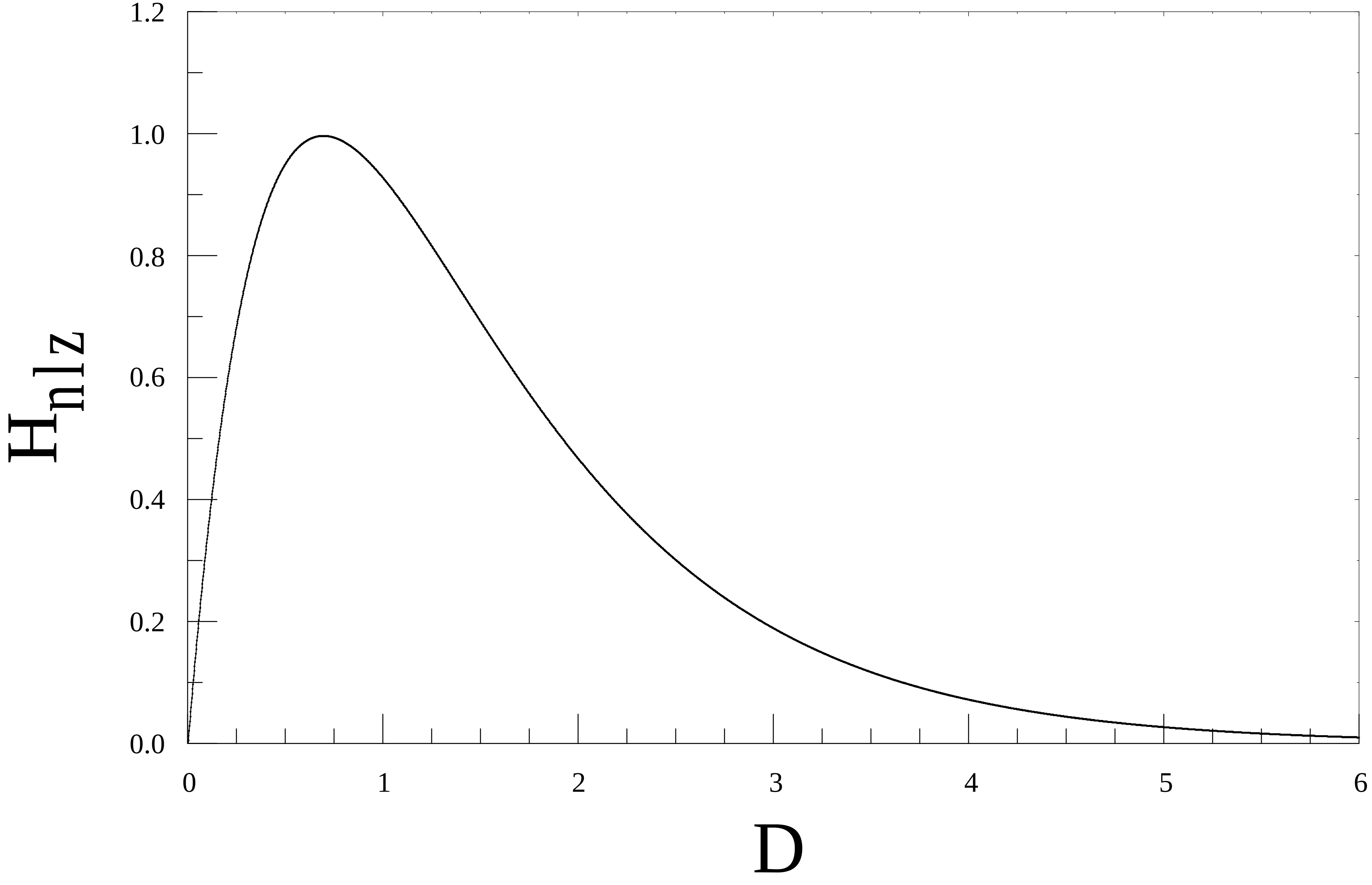

Figure 3 Halterman and Valls

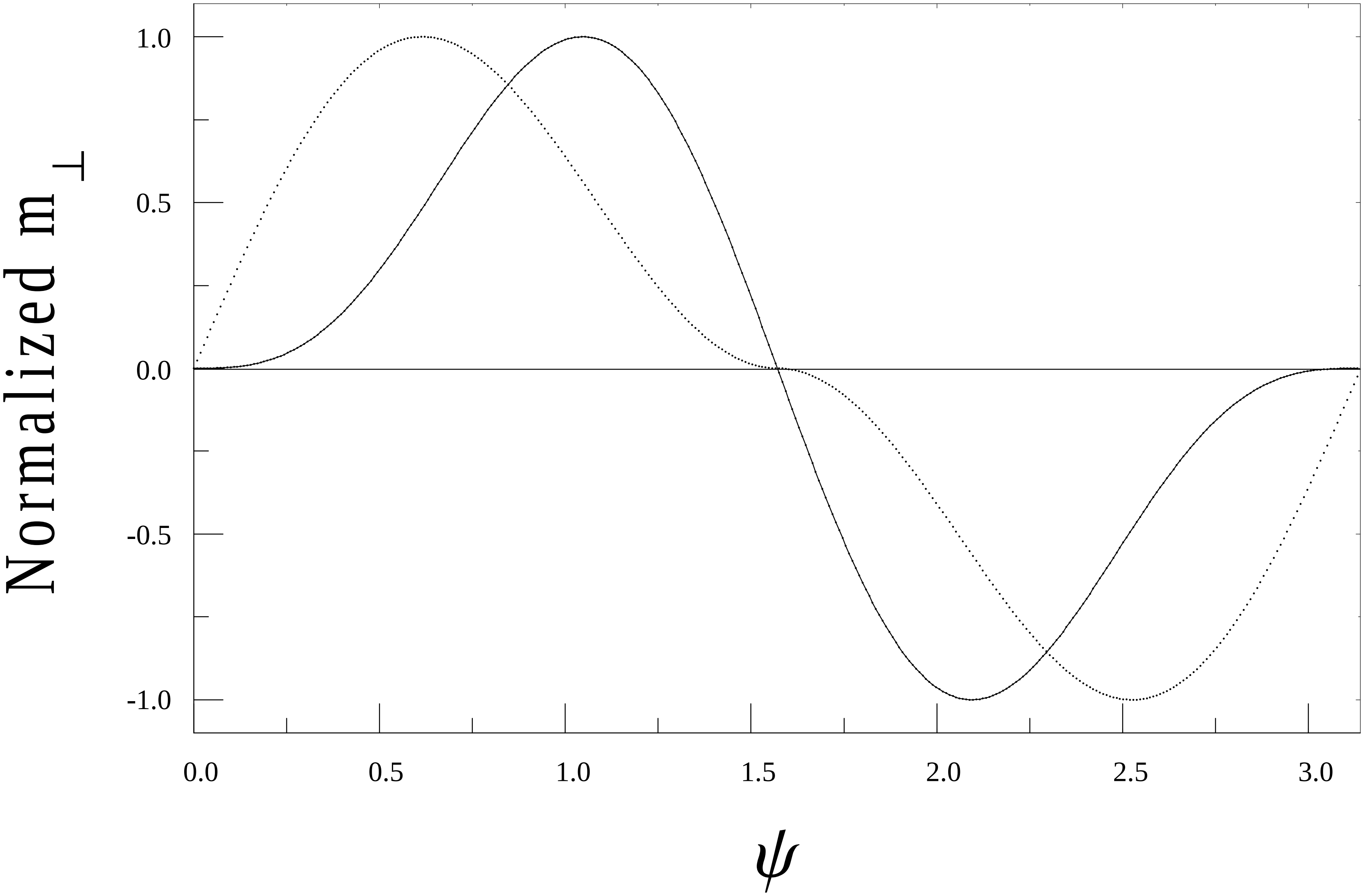

Figure 4 Halterman and Valls